BMC JOURNAL OF SCIENTIFIC RESEARCH
A Multidisciplinary Peer Reviewed Research Journal
ISSN: 2594-3421 (Print), 2773-8191 (Online)

Prediction of Earthquakes in Nepal and the Adjoining Regions Using LSTM

Manoj Aryal, Ram Krishna Tiwari*, Harihar Paudyal

Birendra Multiple Campus, Tribhuvan University, Bharatpur, Chitwan, Nepal
*Corresponding Author: ram.tiwari@bimc.tu.edu.np
ORCID: 0000-0003-4519-0365 (RKT), 0000-0003-2651-9022 (HP)

Received: September 7, 2024, Accepted: Dec. 3, 2024
DOI: https://doi.org/10.3126/bmcjsr.v7i1.73058

Abstract

This study applies Long Short-Term Memory (LSTM) model to predict earthquake magnitudes in the frequently earthquake-affected Himalayan country Nepal and the adjoining region. The seismic data on the mb scale, from September 1964 to August 2024, were taken from the International Seismological Centre (ISC) catalogue, spanning rectangular boundary of latitudes 26.30°N to 30.50°N and longitudes 80.00°E to 88.30°E. The methodology involved extensive data preprocessing, feature engineering, and the implementation of a deep learning model. The LSTM network demonstrated moderate predictive power, achieving a Mean Absolute Error (MAE) of 0.2789, Root Mean Square Error (RMSE) of 0.3728, and coefficient of determination (R^2) score of 0.4294. The model effectively captured overall seismic trends and showed consistent performance over time. A limitation of the model is its tendency to predict magnitudes within the range of 3.5 to 5.0, resulting in the underestimation of strong earthquakes and slight overestimation of weaker ones.

Keywords LSTM, neural networks, feature engineering, deep learning model, seismic trends

1. Introduction

Nepal and the adjoining regions are highly prone to earthquakes. This is because it lies along the boundary of two major Indian and Eurasian tectonic plates. The collision between those plates primarily shapes the Himalayan region's tectonics. The collision started about 50 million years ago, and it still occurs up to date (Dwivedi & Chamoli, 2022; Ni, 1989; R. K. Tiwari, 2023). The immense pressure from this ongoing collision causes the Earth's crust to buckle, fold, and thrust upwards, forming the Himalayan Mountain range. This tectonic activity also leads to frequent earthquakes as the crust adjusts to the immense forces at play (Gupta et al., 2021; Thakur, 2004; R. K. Tiwari & Paudyal, 2023b, 2024b).

Significant tectonic features in the Himalayas are the Main Central Thrust (MCT), Main Boundary Thrust (MBT), Main Frontal Thrust (MFT), and South Tibetan Detachment (STD) (L. Bai et al., 2016; R. K. Tiwari, 2023; R. K. Tiwari et al., 2024). The MCT marks the boundary between the higher Himalaya and lesser Himalaya, the MBT separates the Lesser Himalaya (Middle Himalaya) from the Siwalik Hills, and the MFT

lies at the foothills of the Himalayas, demarcating the boundary between the Siwalik Hills and the Indo-Gangetic Plain (Feng et al., 2017; Mugnier et al., 1994; Sinha-Roy, 1982; R. K. Tiwari & Paudyal, 2020, 2022, 2024a). The STD is a low-angle fault zone that forms the northern boundary of the Himalayas. These tectonic structures play a crucial role in the region's seismicity (Bilham, 2019; Zhang et al., 2020). Historical data shows that the Himalayas have experienced numerous devastating earthquakes, including the Gorkha earthquake in 2015 in Nepal (Khan et al., 2016; Thapa et al., 2023; R. K. Tiwari & Paudyal, 2023a; R. K. Tiwari & Paudyal, 2021)

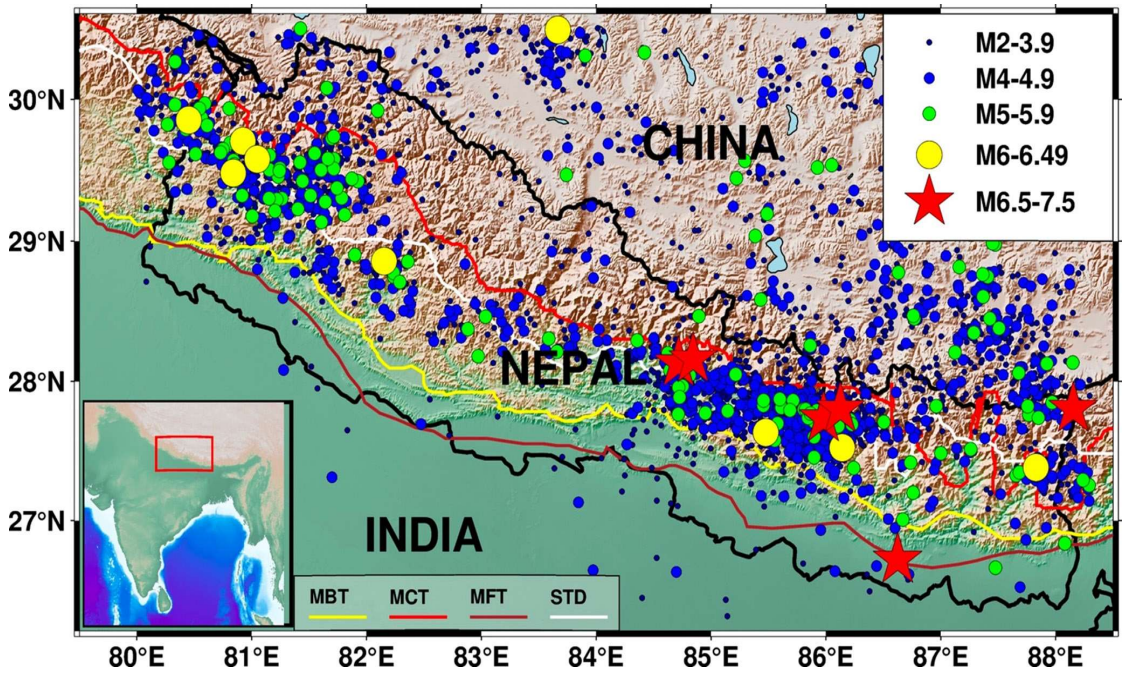

Figure 1. Map of Nepal and adjoining regions showing earthquake epicenters from September 1964 to July 2024, categorized by magnitude: M2-3.9 (dark blue circles), M4-4.9 (blue circles), M5-5.9 (green circles), M6-6.49 (yellow circles), and M6.5-7.5 (red stars). Tectonic features include the Main Boundary Thrust (MBT, yellow line), Main Central Thrust (MCT, red line), Main Frontal Thrust (MFT, brown line), and South Tibetan Detachment (STD, white line). An inset map provides a regional context.

Understanding and predicting seismic events in this region is crucial for minimizing loss of life and property damage. Researchers have extensively studied the spatial and temporal patterns of earthquake occurrences in the Himalayas. Bilham (2004) provided a comprehensive overview of seismic activity in the Himalayan arc, emphasizing the role of large thrust earthquakes in shaping regional tectonics. Earthquake magnitude estimation has been a critical area of research, with studies like Pandey et al. (1995), investigating the relationship between body wave magnitude (mb) and moment magnitude (Mw) for Himalayan earthquakes has been instrumental in establishing standardized approaches to magnitude determination. Pandey et al. (1999) focused on

specific segments of the Himalayas, analyzing recurrence intervals and seismic gaps. Avouac et al. (2006) combined GPS data with historical earthquake records to model strain accumulation and release along fault lines, offering valuable insights into the complex nature of Himalayan tectonics.

Recent advancements in machine learning techniques, particularly Long Short-Term Memory (LSTM) networks, have opened new avenues for earthquake prediction. LSTM networks, a type of recurrent neural network (RNN), are designed to handle sequential data and capture long-term dependencies, making them well-suited for time series prediction tasks (Graves, 2012). Several studies have applied LSTM models to predict seismic activities, highlighting their advantages in capturing temporal dependencies (González et al., 2019; K et al., 2019). Berhich et al. (2023) advanced the field by incorporating attention-based LSTM models for large earthquake prediction, while Hsu & Pratomo (2022) explored LSTM networks for predicting ground acceleration.

Wang et al. (2020) contributed significantly to spatio-temporal data mining using LSTM networks, emphasizing the importance of capturing complex seismic patterns. Hasan Al Banna et al. (2021) applied LSTM models in the context of Bangladesh, highlighting regional challenges in data quality and availability. Recent studies have also focused on enhancing LSTM models through advanced data preprocessing and feature engineering techniques (T. Bai & Tahmasebi, 2022).

This study aims to develop a robust LSTM-based model for earthquake prediction in the Himalayan region, focusing on Nepal and its adjoining areas. The research utilizes historical seismic data from September 1964 to August 2024, employing the mb magnitude scale. The primary objectives are to build and evaluate an LSTM model for earthquake prediction, assess its performance using metrics such as R^2, MAE, RMSE, MSE, and accuracy, and identify patterns or trends in predicted seismic activity (Monterrubio-Velasco et al., 2024).

2. Data and methodology

Earthquake data for Nepal and the adjoining regions (Latitude range from 26.30°N to 30.50°N and Longitude range from 80.00°E to 88.30°E) from September 1964 to August 2024 was taken from the International Seismological Centre (ISC) catalogue (Di Giacomo et al., 2015, 2018). We have made every effort to use uniform procedures of magnitude determination throughout the entire period of the catalogue. The re-computation of the surface wave MS and short-period body-wave mb values benefitted from new hypocentres. The ISC provides a comprehensive and standardized dataset of earthquake occurrences worldwide. The raw data from the ISC catalogue underwent several preprocessing steps to ensure its suitability for the LSTM model. The raw data from the ISC catalogue contains additional metadata, such as event identification numbers, author's names, station codes, and phase data, which are not required for this study.

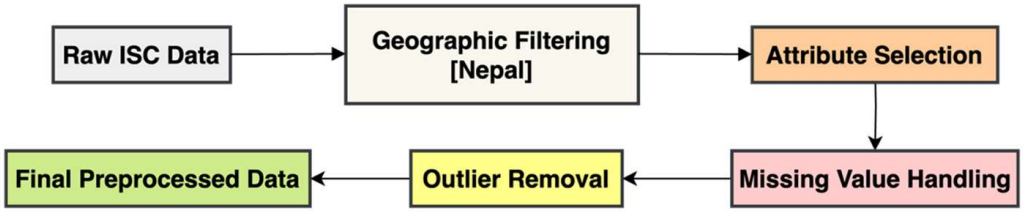

Figure 2. Raw ISC data preprocessing pipeline

Data cleaning involved handling missing values, outliers, and inconsistencies. Additionally, temporal and spatial filtering will be applied to focus on significant events and reduce noise in the data. The final dataset retained key attributes, which are crucial for training the LSTM model, as outlined in Table 1.

Table 1. Attributes of Earthquake Dataset into LSTM model

Attribute	Description	Unit
DATE & TIME	Date and Time of earthquake occurrence	YYYY-MM-DD HH:MM:SS
LON	Longitude of epicenter	Degrees
LAT	Latitude of epicenter	Degrees
DEPTH	Depth of hypocenter	Kilometers
MAG	Earthquake magnitude	mb scale

To prepare the data for input into the LSTM model, it is structured as a time series with multiple features. The feature engineering process involved creating the following features:

Table 2. Features Used for Data Structuring into LSTM Model

Feature Type	Usage
Temporal	Days since the last earthquake, Day of the year, Month
Spatial	Latitude, Longitude, Depth
Magnitude	Current earthquake Magnitude, Average magnitude of last 5 earthquakes

The data was organized into sequences, with each sequence representing a window of past events used to predict the magnitude of the next event. The final feature set for the LSTM model included the following: latitude (LAT), longitude (LON), depth (DEPTH), days since the last event (Days_Since_Last), day of the year (Day_of_Year), month (Month), and the rolling mean of the magnitudes (MAG_Rolling_Mean).

After feature engineering, the data underwent further preparation steps to optimize it for the LSTM model. These steps included feature scaling using a MinMaxScaler to normalize all features to a range between 0 and 1, ensuring equal contribution of features and improving model convergence. 80% of the dataset was provided for training and

the remaining 20% for testing, allowing for proper model evaluation on unseen data. Finally, the provided dataset was reshaped to meet the LSTM model's requirements, resulting in a training data shape of (2268, 1, 7) and a test data shape of (568, 1, 7), representing the number of samples, time steps, and features respectively.

Table 3. Data Shapes After Preprocessing

Dataset	Shape	Description
Training	(2268, 1, 7)	2268 samples, 1-time step, 7 features
Testing	(568, 1, 7)	568 samples, 1-time step, 7 features

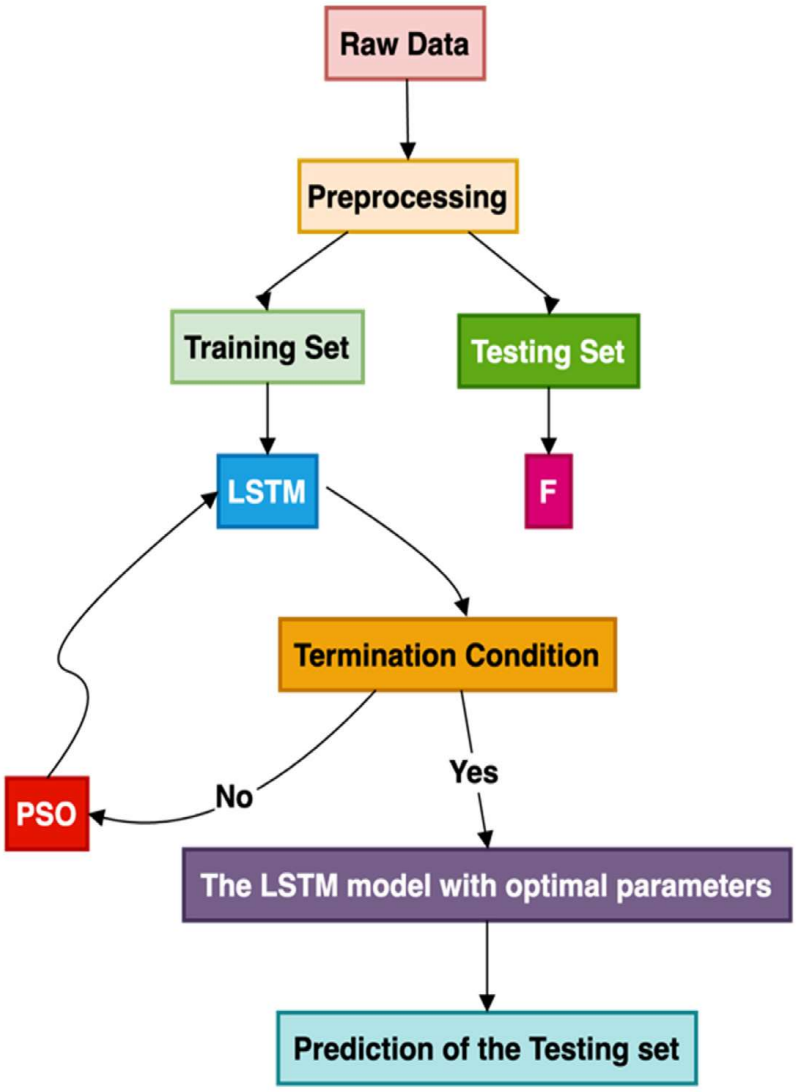

Figure 3. Flowchart of LSTM

The model was compiled with the following specifications:

Table 4. Testing Parameters Metrics

Hyper-parameter	Value
Learning Rate	0.001
Batch size	32
Epochs	100
Optimizer	Adam
Loss Function	MSE
Validation split	20% of training data

A 5-fold cross-validation strategy was employed to ensure robust performance evaluation and to reduce the likelihood of overfitting, ensuring the model generalizes well to unseen data. 80% of the dataset was provided for testing and the remaining 20% for testing with the training set further divided for cross-validation. The following measures were used to assess the model's performance:

Mean Absolute Error (MAE): $\mathrm{MAE} = \frac{1}{n}\sum_{i=1}^{n} | y_i - \hat{y}_i |$

Root Mean Square Error (RMSE): $\mathrm{RMSE} = \sqrt{\frac{1}{2}\sum_{i=1}^{n}\left(y_i - \hat{y}_i \right)^2}$

Coefficient of determination (R^2) Score: $R^2 = 1 - \frac{\sum_{i=1}^{n}\left(y_i - \hat{y}_i \right)^2}{\sum_{i=1}^{n}\left(y_i - \bar{y} \right)^2}$

True values are denoted by y_i, predicted values by $\hat{y}_i$, and mean of the true values by $\bar{y}$.

3. Results and discussion

The presence of overlapping data in Figure 4 indicates that both training and test data capture the overall distribution of the original dataset, ensuring that the model is trained and tested on a realistic representation of seismic activity in Nepal. This alignment is critical in the LSTM model's ability to generalize and predict earthquake magnitudes accurately. The graph also suggests that the model was exposed to a broad range of magnitudes, including moderate to strong earthquakes, allowing for a balanced evaluation of predictive accuracy across varying magnitudes.

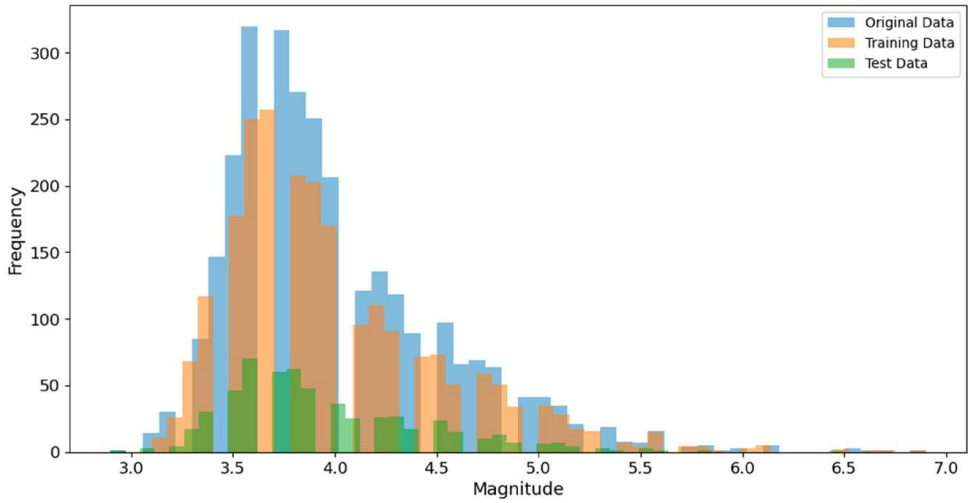

Figure 4. Distribution of magnitudes

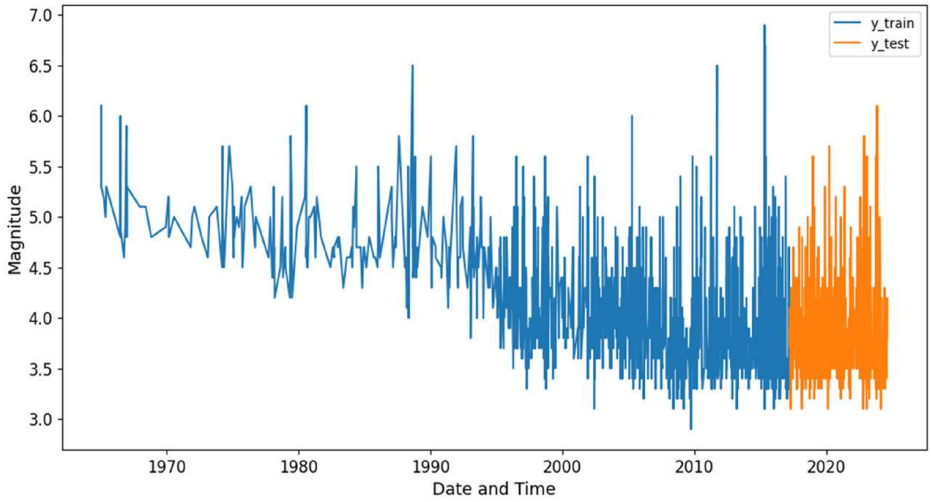

Figure 5. Train and Test Magnitude over time

Figure 5 presents the seismic activity recorded over several decades, showcasing both the training and test datasets used in our LSTM-based prediction model. The blue line represents the training data, encompassing a longer historical period, while the orange line indicates the more recent test data. Throughout the timeline, we observe significant fluctuations in earthquake magnitudes, ranging primarily from 3.0 to 7.0 on the scale. Notable spikes in the graph correspond to major seismic events that have impacted the region. A striking feature of this visualization is the apparent increase in data density over time, particularly evident from the 1990s onward. This trend likely reflects advancements in seismic monitoring technology and more comprehensive data collection practices, rather than necessarily indicating an increase in seismic activity itself. The graph effectively captures the complex and variable nature of Nepal's seismic history, highlighting periods of relative quiescence interspersed with instances of intense activity.

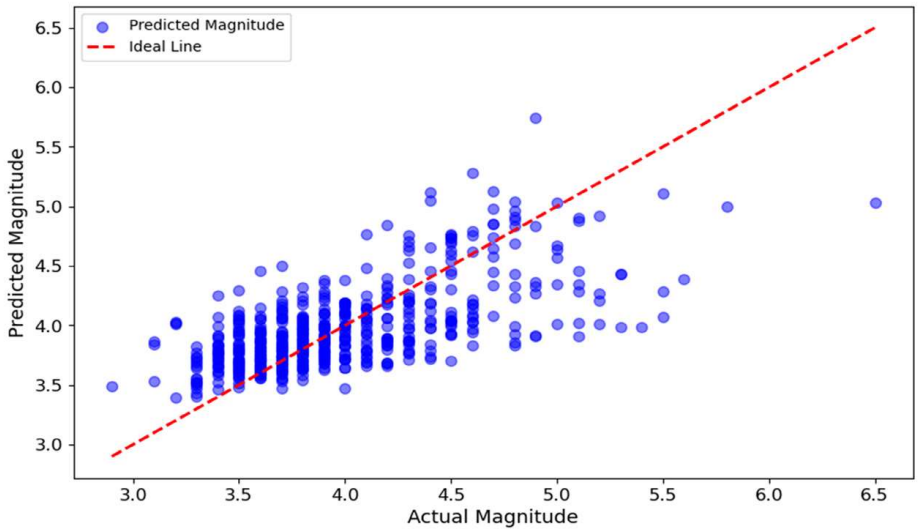

Figure 6. Actual vs Predicted Earthquake Magnitude Scatter plot

In Figure 6, a positive correlation between actual and predicted magnitudes is evident, indicating that the model captures the general trend of earthquake intensities. However, the model's predictions tend to fall within a narrower range compared to actual observations, particularly for extreme events. For earthquakes with magnitudes below 4.0, the model shows a tendency to slightly overestimate, while it often underestimates magnitudes for events above 5.0.

The model demonstrates its best performance for earthquakes in the 4.0 to 5.0 magnitude range, where predictions cluster more closely around the ideal prediction line. These observations highlight the model's strengths in predicting moderate earthquakes while also revealing areas for potential improvement in capturing the full spectrum of seismic event intensities.

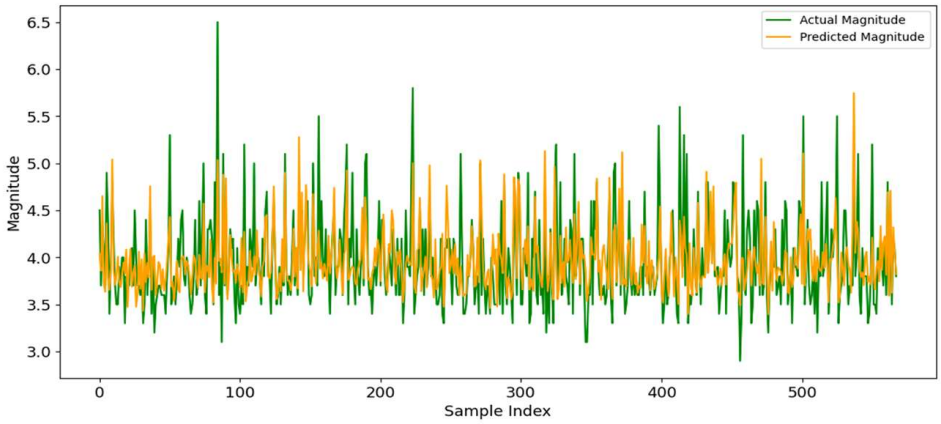

Figure 7. Line graph comparing actual versus predicted magnitudes for a 600 sample index. The green line represents the actual magnitudes, while the orange line represents the magnitudes predicted by the model.

Figure 7 presents a line graph comparing actual and predicted earthquake magnitudes across a sample index. This visualization allows for a direct comparison between observed and predicted values over a sequence of earthquake events. The graph reveals that the model generally captures the overall trend of magnitude fluctuations, with predictions closely following the actual values for many instances. However, there are notable discrepancies, particularly for higher magnitude events where the model tends to underestimate the peak values.

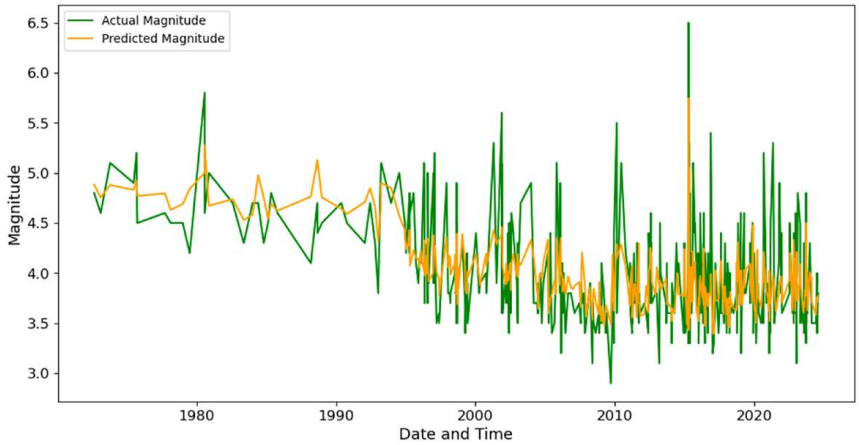

Figure 8. Line graph comparing actual versus predicted magnitudes of Entire Test Size

Figure 8 expands the view to display the model's performance specifically for the entire test dataset. This broader perspective offers a comprehensive view of the model's predictive capabilities across a range of seismic events on unseen data. The graph spans the full test set, providing a clearer picture of how well the model generalizes to new data points. It becomes evident that while the model maintains its ability to follow general trends, its struggle with higher-magnitude earthquakes persists across the larger dataset.

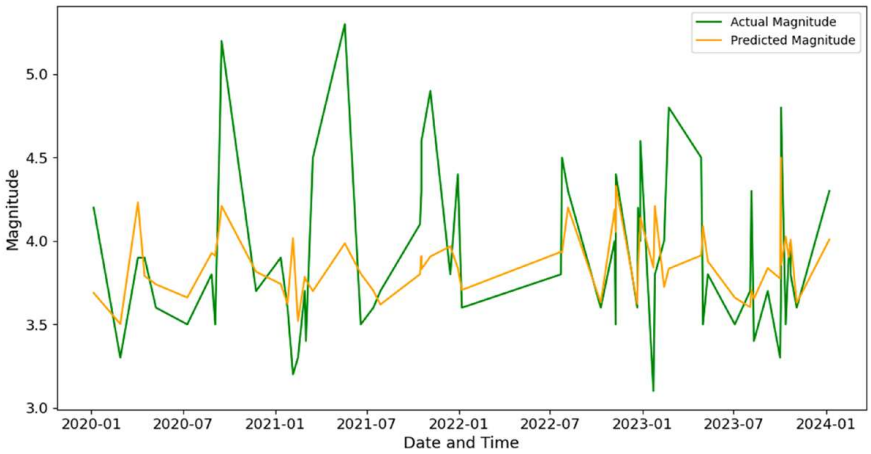

Figure 9. Line graph comparing actual versus predicted magnitudes from January 2020 to January 2024.

Figure 9 narrows the focus to a recent period, showing actual and predicted earthquake magnitudes from January 2020 to January 2024. This timeframe is particularly valuable for assessing the model's performance on more current seismic data trends and its potential reliability for future predictions. The graph demonstrates that the model's ability to capture general trends remains consistent even with recent data. However, it also confirms the limitation in accurately predicting higher magnitude events observed in the previous figures. The model's predictions tend to fall within a narrower range in all the observed periods (approximately 3.5 to 5.0) compared to the actual magnitudes, which exhibit more extreme values. This leads to an underestimation of larger earthquakes (above 5.5 magnitude) and a slight overestimation of very low magnitude events (below 3.5). The model's performance appears consistent across time, without significant degradation or improvement over time.

Notably, there's clear evidence of the variation between actual magnitude and predicted magnitude which may be due to insufficient training data or an imbalance caused by a higher prevalence of lower-magnitude events.

Performance evaluation

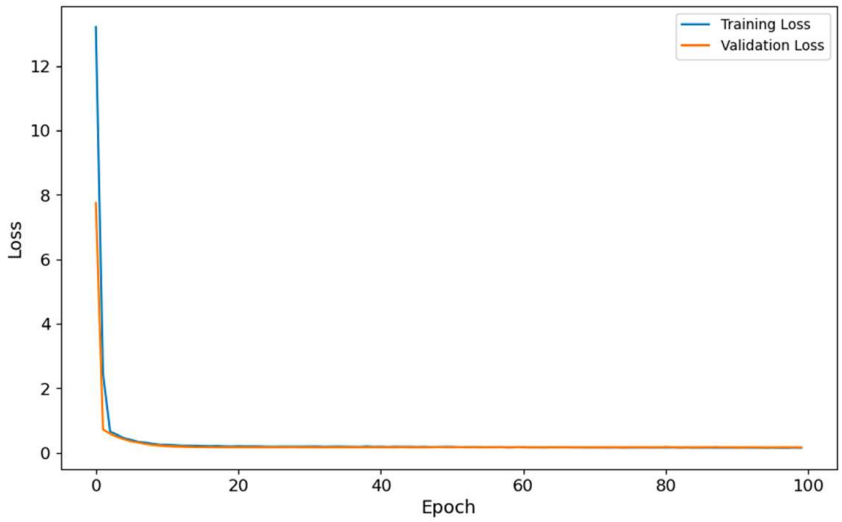

Figure 10. Fitting curves of LSTM training process showing Model Loss over Epochs

Initial epochs showed the training and validation loss of the model decreased and then stabilized later, indicating successful learning. It seems that the model did not over fit the training set based on the close alignment of the validation and training loss curves. The Mean Absolute Error of 0.2789 indicates that, on average, the model's predictions deviate from the testing earthquake magnitudes by approximately 0.28 units on the mb scale. RMSE of 0.3728 provides a measure of the standard deviation of the residuals. The R^2 score of 0.4294 suggests that the model explains about 42.94% of the variability in earthquake magnitudes.

To ensure model robustness and to account for potential data variability, a 5-fold cross-validation approach was implemented. The cross-validation results are consistent with the performance on the test set, indicating that the performance of the model remains consistent across various data subsets. The slightly higher R-squared value in cross-validation (0.4468) compared to the test set (0.4294) suggests that the model's predictive power might be slightly better when evaluated across multiple data splits.

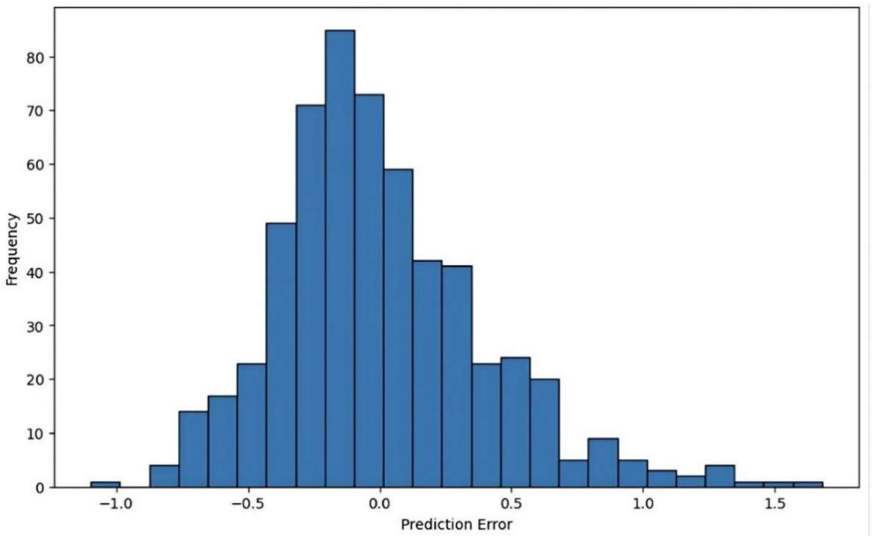

Figure 11. Histogram of Prediction Errors

The errors exhibit a central tendency around zero, indicating that the model doesn't display a strong bias towards over- or under-prediction. This balanced performance is further supported by the roughly symmetric distribution, suggesting an equal likelihood of overestimation and underestimation. This error is consistent with the reported Mean Absolute Error (MAE) of 0.2789, with most errors falling within the range of -0.5 to 0.5 magnitude units. While there are instances of larger errors beyond ±1.0 magnitude units, these occurrences are relatively infrequent. This error distribution pattern demonstrates the model's overall reliability in predicting earthquake magnitudes, while also highlighting areas for potential improvement in reducing the frequency of larger errors.

Table 5. LSTM Model Summary consisting of the type of each layer, their output shapes, and the number of parameters

Layer (type)	Output Shape	Param #
lstm (LSTM)	(None, 64)	18,432
dropout (Dropout)	(None, 64)	0
dense (Dense)	(None, 32)	2080
dense_1 (Dense)	(None, 1)	33

The model followed a sequential structure, beginning with an LSTM layer that outputs 64 units. This layer contains 18,432 parameters and was crucial for capturing the temporal patterns and long-term relationships in the earthquake time-series data. After the LSTM, a dropout layer was added to avoid over fitting, which did not introduce any additional parameters but helped improve the model's generalization ability by randomly disabling certain neurons during training. The model was further refined with a dense layer comprising 32 units and 2,080 parameters. This fully connected layer transforms the features learned by the LSTM layer, contributing model predicting the target variable more accurately. Future earthquake magnitude predictions were made using a dense layer with a single unit in the final output layer. This layer had 33 parameters and was the model's output for regression tasks.

Overall, the model consisted of 20,545 trainable parameters and employed an optimizer with 41,092 parameters to adjust the weights during training. The total parameter count was 61,637. The structure and parameter count were optimized for handling the time-series nature of earthquake data, demonstrating an efficient approach to predicting seismic activity in Nepal and the adjoining regions. In recent past study, smaller magnitude earthquakes, magnitude between 5 to 5.5, were forecast more accurately for the Himalayan region by neural networks models (Prakke & Pradeep Kumar, 2024).

4. Conclusion

This study developed and evaluated an LSTM neural network model for predicting earthquake magnitudes in the Himalayan region of Nepal, utilizing seismic data from the ISC catalogue. The model demonstrated potential success, achieving a coefficient of determination (R^2) score of 0.4294, indicating its ability to capture overall seismic trends. While the model maintained consistent performance and successfully identified general patterns, it struggled with predicting extreme events, particularly high-magnitude earthquakes. The model's tendency to predict within a narrower range (3.5 to 5.0) led to the underestimation of high-magnitude events and a slight overestimation of low-magnitude ones. The model's ability to explain about 42.94% of the variability in earthquake magnitudes is significant, given the complex and chaotic nature of seismic events. This performance suggests that machine learning approaches have considerable potential in advancing our understanding of seismic patterns, even if they cannot predict individual events with high accuracy. LSTMs can be integrated with geological and geophysical data, including GPS measurements, stress-strain analysis, and tectonic plate velocities, to enhance the understanding of seismicity in the Himalayas.

Software resources

The experimental setup for this study involved using Python 3.12.5 as the programming language. The study utilized several libraries and packages, including TensorFlow 2.17, Keras 3.5.0, Pandas 2.2.2, NumPy 2.0.1, scikit-learn 1.5.1, Matplotlib 3.9.2, and PyGMT 0.12.0. JupyterLab Desktop 4.2.1 was used as the development environment.

In particular, PyGMT was used for plotting earthquake data on the map of Nepal, digitally adding a base map for enhanced visualization.

References

Avouac, J. P., Ayoub, F., Leprince, S., Konca, O., & Helmberger, D. V. (2006). The 2005, Mw 7.6 Kashmir earthquake: Sub-pixel correlation of ASTER images and seismic waveforms analysis. *Earth and Planetary Science Letters*, *249*(3–4), 514–528. https://doi.org/10.1016/j.epsl.2006.06.025

Bai, L., Liu, H., Ritsema, J., Mori, J., Zhang, T., Ishikawa, Y., & Li, G. (2016). Faulting structure above the Main Himalayan Thrust as shown by relocated aftershocks of the 2015 Mw7.8 Gorkha, Nepal, earthquake. *Geophysical Research Letters*, *43*(2), 637–642. https://doi.org/10.1002/2015GL066473

Bai, T., & Tahmasebi, P. (2022). Attention-based LSTM-FCN for earthquake detection and location. *Geophysical Journal International*, *228*(3), 1568–1576. https://doi.org/10.1093/gji/ggab401

Berhich, A., Belouadha, F. Z., & Kabbaj, M. I. (2023). An attention-based LSTM network for large earthquake prediction. *Soil Dynamics and Earthquake Engineering*, *165*, 107663. https://doi.org/10.1016/J.SOILDYN.2022.107663

Bilham, R. (2004). Earthquakes in India and the Himalaya: Tectonics, geodesy and history. *Annals of Geophysics*, *47*(2–3), 839–858.

Bilham, R. (2019). Himalayan earthquakes: A review of historical seismicity and early 21st century slip potential. *Geological Society Special Publication*, *483*(1), 423–482. https://doi.org/10.1144/SP483.16

Di Giacomo, D., Bondár, I., Storchak, D. A., Engdahl, E. R., Bormann, P., & Harris, J. (2015). ISC-GEM: Global instrumental earthquake catalogue (1900-2009), III. Re-computed MS and mb, proxy MW, final magnitude composition and completeness assessment. *Physics of the Earth and Planetary Interiors*, *239*, 33–47. https://doi.org/10.1016/j.pepi.2014.06.005

Di Giacomo, D., Robert Engdahl, E., & Storchak, D. A. (2018). The ISC-GEM earthquake catalogue (1904-2014): Status after the extension project. *Earth System Science Data*, *10*(4), 1877–1899. https://doi.org/10.5194/essd-10-1877-2018

Dwivedi, D., & Chamoli, A. (2022). Seismotectonics and lineament fabric of Delhi fold belt region, India. *Journal of Earth System Science*, *131*(2). https://doi.org/10.1007/s12040-022-01829-w

Feng, W., Lindsey, E., Barbot, S., Samsonov, S., Dai, K., Li, P., Li, Z., Almeida, R., Chen, J., & Xu, X. (2017). Source characteristics of the 2015 MW 7.8 Gorkha (Nepal) earthquake and its MW 7.2 aftershock from space geodesy. *Tectonophysics*, *712–713*, 747–758. https://doi.org/10.1016/j.tecto.2016.02.029

González, J., Yu, W., & Telesca, L. (2019). *Earthquake Magnitude Prediction Using Recurrent Neural Networks*. 22. https://doi.org/10.3390/iecg2019-06213

Graves, A. (2012). *Supervised Sequence Labelling with Recurrent Neural Networks. Studies in Computational Intelligence.* https://doi.org/10.1115/ices2001-140

Gupta, S. K., Roy, P. N. S., & Pal, S. K. (2021). Scale invariance behavior for pre and post-2015 Nepal Gorkha earthquake GPS time series based on fractal analysis. *Chaos, Solitons and Fractals*, *152*, 111341. https://doi.org/10.1016/j.chaos.2021.111341

Hasan Al Banna, M., Ghosh, T., Taher, K. A., Kaiser, M. S., & Mahmud, M. (2021). An earthquake prediction system for Bangladesh using deep long short-term memory architecture. In *Lecture Notes in Networks and Systems* (Vol. 185). https://doi.org/10.1007/978-981-33-6081-5_17

Hsu, T. Y., & Pratomo, A. (2022). Early peak ground acceleration prediction for on-site earthquake early warning using LSTM neural network. *Frontiers in Earth Science*, *10*(July), 1–17. https://doi.org/10.3389/feart.2022.911947

K, V., Bhandarkar, T., Satish, N., Sridhar, S., Sivakumar, R., & Ghosh, S. (2019). Earthquake trend prediction using long short-term memory RNN. *International Journal of Electrical and Computer Engineering (IJECE)*, *9*(2), 1304–1312. https://doi.org/10.11591/ijece.v9i2.pp1304-1312

Khan, P. K., Mohanty, S. P., Sinha, S., & Singh, D. (2016). Occurrences of large-magnitude earthquakes in the Kachchh region, Gujarat, western India: Tectonic implications. *Tectonophysics*, *679*, 102–116. https://doi.org/10.1016/j.tecto.2016.04.044

Monterrubio-Velasco, M., Callaghan, S., Modesto, D., Carrasco, J. C., Badia, R. M., Pallares, P., Vázquez-Novoa, F., Quintana-Ortí, E. S., Pienkowska, M., & de la Puente, J. (2024). A machine learning estimator trained on synthetic data for real-time earthquake ground-shaking predictions in Southern California. *Communications Earth and Environment*, *5*(1), 1–11. https://doi.org/10.1038/s43247-024-01436-1

Mugnier, J. L., Huyghe, P., Chalaron, E., & Mascle, G. (1994). Recent movements along the main boundary thrust of the Himalayas: Normal faulting in an over-critical thrust wedge? *Tectonophysics*, *238*(1–4), 199–215. https://doi.org/10.1016/0040-1951(94)90056-6

Ni, J. F. (1989). Active tectonics of the Himalaya. *Proceedings of the Indian Academy of Sciences - Earth and Planetary Sciences*, *98*(1), 71–89. https://doi.org/10.1007/BF02880377

Pandey, M. R., Tandukar, R. P., Avouac, J. P., Lavé, J., & Massot, J. P. (1995). Interseismic strain accumulation on the Himalayan crustal ramp (Nepal). *Geophysical Research Letters*, *22*(7), 751–754. https://doi.org/10.1029/94GL02971

Pandey, M. R., Tandukar, R. P., Avouac, J. P., Vergne, J., & Héritier, T. (1999). Seismotectonics of the Nepal Himalaya from a local seismic network. *Journal of Asian Earth Sciences*, *17*(5–6), 703–712. https://doi.org/10.1016/S1367-9120(99)00034-6

Prakke, B., & Pradeep Kumar, R. (2024). Earthquake forecasting in the Himalayan region using neural networks models. *Sadhana - Academy Proceedings in Engineering Sciences*, *49*(1). https://doi.org/10.1007/s12046-023-02398-4

Sinha-Roy, S. (1982). Himalayan main central thrust and its implications for Himalayan inverted metamorphism. *Tectonophysics*, *84*(2–4), 197–224. https://doi.org/10.1016/0040-1951(82)90160-3

Thakur, V. C. (2004). Active tectonics of Himalayan frontal thrust and seismic hazard to Ganga Plain. *Current Science*, *86*(11), 1554–1560. https://doi.org/10.1007/s00531-013-0891-7

Thapa, H. R., Pachhai, S., Aoudia, A., Manu-Marfo, D., Priestley, K., & Mitra, S. (2023). The main Himalayan thrust beneath Nepal and southern Tibet illuminated by seismic ambient noise and teleseismic P wave coda autocorrelation. *Journal of Geophysical Research: Solid Earth*, *128*(8), 1–21. https://doi.org/10.1029/2022JB026195

Tiwari, R. K. (2023). *Multifractal Approach To the Study of Gorkha Earthquake of 25 April, 2015 Nepal*. Institute of science & technology, Tribhuvan University. https://hdl.handle.net/20.500.14540/20818

Tiwari, R. K., Chaudhary, S., Paudyal, H., & Shanker, D. (2024). Identifying seismicity pattern before major earthquakes in the Western Nepal and adjoining region (28.5°N to 31.0°N − 78°E to 82.96°E). *Environmental Earth Sciences*, *83*(15), 1–11. https://doi.org/10.1007/s12665-024-11764-2

Tiwari, R. K., & Paudyal, H. (2020). Geodynamics of Gorkha earthquake (Mw 7.9) and its aftershocks. *Himalayan Physics*, *9*, 103–109. https://doi.org/10.3126/hp.v9i01.40208

Tiwari, R. K., & Paudyal, H. (2022). Frequency magnitude distribution and spatial correlation dimension of earthquakes in north-east Himalaya and adjacent regions. *Geologos*, *28*(2), 115–128. https://doi.org/10.2478/logos-2022-0009

Tiwari, R. K., & Paudyal, H. (2023a). Fractal characteristics of the seismic swarm succeeding the 2015 Gorkha earthquake, Nepal. *Indian Geotechnical Journal*, *53*(4), 789–804. https://doi.org/10.1007/s40098-022-00704-1

Tiwari, R. K., & Paudyal, H. (2023b). Spatial mapping of b-value and fractal dimension prior to November 8, 2022 Doti earthquake, Nepal. *PLOS ONE*, *18*(8), 1–13. https://doi.org/10.1371/journal.pone.0289673

Tiwari, R. K., & Paudyal, H. (2024a). Analysis of the b, p values, and the fractal dimension of aftershocks sequences following two major earthquakes in central Himalaya. *Heliyon*, *10*(2), e24476. https://doi.org/10.1016/j.heliyon.2024.e24476

Tiwari, R. K., & Paudyal, H. (2024b). b-value Estimation and extreme magnitude assessment in the source region of past earthquakes in central Himalaya and vicinity. *Jordan Journal of Earth and Environmental Sciences*, *15*(3), 183–191.

Tiwari, R., & Paudyal, H. (2021). Seismic phases of 25 April 2015 (Mw 7.8) Earthquake and 12 May 2015 (Mw 7.3) earthquake predicted by AK135 Model - A comparison. *Journal of Nepal Physical Society*, *7*(2), 58–64. https://doi.org/https://doi.org/10.3126/jnphyssoc.v7i2.38623

Wang, Q., Guo, Y., Yu, L., & Li, P. (2020). Earthquake prediction based on spatio-temporal data mining: An LSTM network approach. *IEEE Transactions on Emerging Topics in Computing*, *8*(1), 148–158. https://doi.org/10.1109/TETC.2017.2699169

Zhang, L. K., Li, G. M., Cao, H. W., Zhang, Z., Dong, S. L., Liang, W., Fu, J. G., Huang, Y., Xia, X. B., Dai, Z. W., Pei, Q. M., & Zhang, S. T. (2020). Activity of the south Tibetan detachment system: Constraints from leucogranite ages in the eastern Himalayas. *Geological Journal*, *55*(7), 5540–5573. https://doi.org/10.1002/gj.3756